MDPI

Generic Methodology for Field Calibration of Nacelle-Based Wind Lidars

Antoine Borraccino *,†, Michael Courtney † and Rozenn Wagner †

DTU Wind Energy, Technical University of Denmark, Kongens Lyngby 2800, Denmark;
mike@dtu.dk (M.C.); rozn@dtu.dk (R.W.)
*   Correspondence: borr@dtu.dk; Tel.: +45-9351-1124
†   Current address: Risø Campus, Frederiksborgvej 399, Roskilde 4000, Denmark.

Abstract: Nacelle-based Doppler wind lidars have shown promising capabilities to assess power performance, detect yaw misalignment or perform feed-forward control. The power curve application requires uncertainty assessment. Traceable measurements and uncertainties of nacelle-based wind lidars can be obtained through a methodology applicable to any type of existing and upcoming nacelle lidar technology. The generic methodology consists in calibrating all the inputs of the wind field reconstruction algorithms of a lidar. These inputs are the line-of-sight velocity and the beam position, provided by the geometry of the scanning trajectory and the lidar inclination. The line-of-sight velocity is calibrated in atmospheric conditions by comparing it to a reference quantity based on classic instrumentation such as cup anemometers and wind vanes. The generic methodology was tested on two commercially developed lidars, one continuous wave and one pulsed systems, and provides consistent calibration results: linear regressions show a difference of ∼0.5% between the lidar-measured and reference line-of-sight velocities. A comprehensive uncertainty procedure propagates the reference uncertainty to the lidar measurements. At a coverage factor of two, the estimated line-of-sight velocity uncertainty ranges from 3.2% at 3 m·s^{-1} to 1.9% at 16 m·s^{-1}. Most of the line-of-sight velocity uncertainty originates from the reference: the cup anemometer uncertainty accounts for ∼90% of the total uncertainty. The propagation of uncertainties to lidar-reconstructed wind characteristics can use analytical methods in simple cases, which we demonstrate through the example of a two-beam system. The newly developed calibration methodology allows robust evaluation of a nacelle lidar's performance and uncertainties to be established. Calibrated nacelle lidars may consequently be further used for various wind turbine applications in confidence.

Keywords: lidar; calibration; uncertainties; nacelle-mounted; wind turbine; power performance
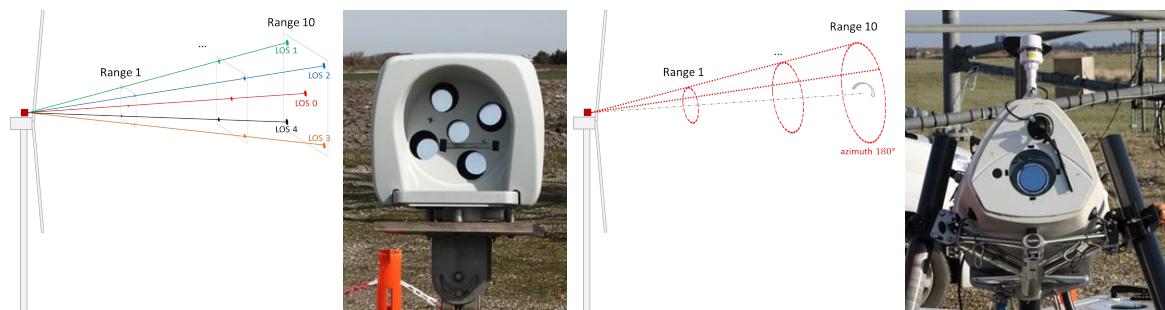
1. Introduction

1.1. Profiling Lidars for Power Performance

The rapid increase in wind turbines' size has created a need for developing new power performance assessment procedures. The effects of wind speed and direction variations—called shear and veer respectively—over the rotor swept area on power curves can no longer be neglected [1]. Measuring the wind at one point, e.g., hub height, has consequently become insufficient.

Light detection and ranging (lidar) is a remote sensing technology addressing this challenge. Its multiple applications have found their way into the wind energy market. Ground-based lidars are presently being used to measure wind profiles [2]. They offer a practical and accurate solution for measuring wind over the entire rotor disk. Even though two-beam nacelle-based lidars completing

horizontal wind speed measurements are unable to estimate the wind shear, they show promising capabilities to assess power performance [3] and obviate the erection of expensive meteorology masts, especially offshore.

A new generation of commercially developed profiling nacelle lidars combine the benefits of both technologies. A wind profiling nacelle lidar probes the wind at multiple heights and distances upstream of a turbine — or downstream for wake measurements — from its nacelle. The commercially available technology ranges from scanning to multi-beam lidar systems, e.g., the Zephir Dual-Mode (ZDM) and the 5-beam Avent Demonstrator (5B) lidars (Figure 1, see details on the measurement principles of both systems in [4,5]).

Figure 1. Two wind profiling nacelle lidar examples: 5-beam Avent Demonstrator (**left**) and Zephir Dual-Mode (**right**).

1.2. The Need for Calibration Procedures

Lidars are measuring instruments. As such, their measurements are uncertain and, formally, can only be traced back to international standards via a calibration. In essence, the main role of a calibration is to transfer the traceability of reference instruments and their uncertainties. Developing commercial applications of lidars demands uncertainty quantification, particularly power performance testing. Indeed, the power curve is the primary characteristic of a wind turbine guaranteeing its production. The fundamental reasons for developing calibration procedures is to ensure the measurements are valid and quantify their accuracy—i.e., trueness and precision—by assigning uncertainties to the measurand.

Doppler wind lidars (DWL) do not measure wind characteristics [6,7] directly. They probe the wind by emitting light through a laser beam and at a known wavelength λ. Atmospheric particles following the wind's motion scatter a fraction of the emitted light back to the lidar, at a frequency Doppler-shifted by $\delta\nu$. Scatterers contained in the lidar probe volume yield a histogram of $\delta\nu$ values. The power spectrum is estimated via spectral analysis—i.e., Fourier transforms—of the electrical signal generated by the photodetector. An algorithm, for instance peak, centroid or maximum likelihood, is applied to characterise the Doppler power spectrum and retrieve a single $\delta\nu$ value. $\delta\nu$ is then converted into a Line-Of-Sight (LOS) velocity V_{LOS}, also called radial wind speed (RWS):

$$V_{LOS} = \frac{\delta\nu \cdot \lambda}{2} \tag{1}$$

Wind characteristics are finally estimated by combining multiple V_{LOS} measurements according to an assumed flow model—e.g., horizontally homogeneous for ground-based lidars using Vertical Azimuth Display, see [8,9]. Depending on the employed flow model, profiling nacelle lidars can reconstruct wind speed (WS) and direction (WD), vertical shear, veer, etc.

From first principles (Equation (1)), the LOS velocity is sometimes assumed to be an 'absolute' measurement, in the sense it is derived from well-known physics theory and thus has a negligible uncertainty.

Most modern Doppler wind lidars operate at a wavelength in the infra-red (IR) region, of ≈1560 nm. The laser wavelength is certified to be within ±1 nm corresponding to a V_{LOS} uncertainty <0.01 m·s^{-1}. Yet, spectral broadening due to probe volume effects (aerosol gradients, presence of inhomogeneous wind structures, etc.) [7] and the chosen Doppler frequency shift estimation method create imperfections in lidar V_{LOS} measurements: the shape of Doppler spectra in atmospheric conditions is far from ideal Gaussian or Dirac distributions that are obtained under controlled conditions in a laboratory with a hard target (e.g., moving belt, rotating wheel) or in a wind tunnel. These two arguments contradict the assumption of lidar V_{LOS} being measured 'absolutely'. Unless all the uncertainties of components (optical, mechanical, software) upstream of the V_{LOS} estimation are thoroughly assessed by certified bodies, the only way to quantify the accuracy of V_{LOS} is to compare it to a calibrated reference. In practice, due to the length of the lidar probe, this is only possible through field measurements using for instance calibrated cup anemometers. Then, at the reconstructed wind characteristics level, the flow model inadequacy introduces errors due to e.g., terrain effects, thermal stability, etc. Note that eliminating flow model assumptions and measuring a 3D wind vector is however possible using collocated synchronised V_{LOS} measurements (WindScanner [10] or multi-static systems). For all those reasons, field calibration procedures of lidars are required, at a minimum for power performance applications.

Calibrated measurements are traceable to international standards when they relate to a reference quantity (itself traceable to the SI). The *International Vocabulary of Metrology*, VIM [11], provides definitions of terms in the field of measurements. According to the VIM, a calibration is an:

> *operation that, under specified conditions, in a first step, establishes a relation between the quantity values with measurement uncertainties provided by measurement standards and corresponding indications with associated measurement uncertainties and, in a second step, uses this information to establish a relation for obtaining a measurement result from an indication.*

Additionally, the *Guide to the expression of Uncertainty in Measurement*, GUM [12], suggests analytical methodologies for assessing uncertainties based on the law of propagation of uncertainties.

In this study we attempt to answer the following research questions:

1. Can (nacelle-based) wind lidars be calibrated via a generic procedure, independent of the lidar type or design?
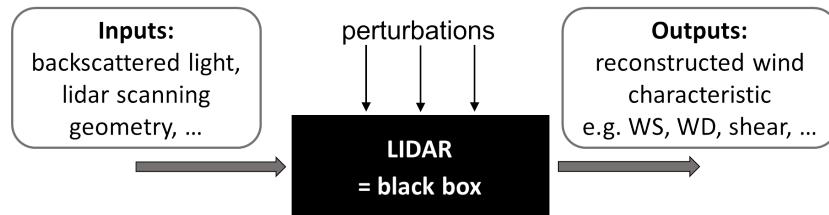2. How to assess lidar measurement uncertainties?

The use of profiling lidars in power performance and need for calibration procedures were first introduced. In Section 2, two plausible concepts for field calibration of nacelle lidars—so-called 'black' and 'white box' approaches—are discussed. The principles of the generic methodology are detailed in Section 3. Section 4 shortly introduces the calibration of the beam positioning quantities. Section 5 focuses on the calibration and uncertainty quantification of the main input of the lidar reconstruction algorithms: the line-of-sight velocity. Calibration results are illustrated with the examples of the 5-beam Avent Demonstrator and ZephIR Dual-Mode lidar units (Figure 1) that have been calibrated during campaigns in 2014–2015 at DTU's test site for large wind turbines, Høvsøre, Denmark. The propagation of inputs uncertainties to lidar-reconstructed wind characteristics is investigated in Section 6 via the simple case of a two-beam lidar system. Finally, we discuss several aspects of the generic methodology, in particular the prevailing uncertainty sources, the question of repeatability, its limitations and how it could be improved.

2. Two Plausible Calibration Concepts: The White- or the Black-Box

In this section, considering the different levels of measurands in a wind lidar, two different calibration concepts are identified where the lidar is regarded either as a 'black' or a 'white' box. We then argue why the white box methodology presents the highest degree of genericity and further detail its principles and steps.

2.1. Black Box

The 'black box' calibration is a direct comparison of the reconstructed wind characteristics with the corresponding reference quantity. Using this approach, the lidar is seen as a black box, a system where the knowledge of the transfer function between inputs and outputs is not relevant or not necessary (Figure 2).

Figure 2. Black box lidar concept.

The wind speed calibration of ground-based lidars is an example of a black box calibration: lidar-estimated horizontal wind speeds (HWS) are compared to reference anemometers placed at multiple heights on a met. mast [13]. For profiling nacelle lidars, the measurement setup of a black box calibration would require:

- **for horizontal wind speed and wind direction:**

  - lidar placed on a platform high enough to allow the beam(s) to not be blocked by the ground in order for the reconstruction algorithm to be available. High stiffness of the tower is required to avoid significant deflections causing the lidar beams to constantly move and sense winds in locations unacceptably far from the reference instruments. This is the reason why we do not recommend calibrating lidars mounted on the nacelle of on an operating wind turbine. The beam perturbations would depend on both the turbine and the actual wind distribution during the testing period. Consequently the repeatability of the calibration would be seriously impaired and the uncertainties increased. For modern wind turbines, the rotor diameter D_{rot} is $\sim$100 m. Power performance standards (IEC 61400-12-1, [14]) require to measure the free wind at an upstream distance of $2.5D_{rot}$. With a cone or half-opening angle of $\alpha = 15°$, the height of the platform should therefore be $>2.5D_{rot} \tan \alpha \approx 67$ m. In addition, a minimum height should be considered to account for the lidar probe volume and avoid sensing highly inhomogeneous and turbulent winds too close to the ground;
  - a mast with reference instruments (e.g., cup or sonic anemometers, wind vanes) mounted at the location where the lidar-reconstructed wind characteristics are estimated. For a two-beam lidar system, such a location may be at the point directly in between the two beam positions, or formally anywhere between the two beams (see Section 6.2);
  - accurate detection of the lidar beam or centreline, in order to position the reference instruments appropriately. This may be extremely difficult to achieve, particularly if no beam is physically present at the centre of the scanning pattern.

- **for vertical wind shear and veer**: reference wind speed and direction instruments located at several heights ranging between the minimum and maximum measurement heights of the lidar, e.g., from 10 m to 150 m.

In practice, the described example setup makes the black box calibration an unrealistic approach for nacelle-based lidars. Such a setup would be extremely expensive, hard to find or develop, and lidar-specific.

2.2. White Box

An alternative methodology to the black box consists in calibrating the reconstruction algorithms' inputs. This method will be further referred to as 'white box' calibration. These inputs are V_{LOS} along the different LOS and beam localisation quantities [15]. The white box calibration requires knowledge of the reconstruction algorithms and being able to:

- calibrate the LOS positioning: e.g., by calibrating the lidar's internal inclinometers (if any), by verifying the geometry of the trajectory (opening angle between each LOS and the optical centreline), by verifying the measurement range;
- calibrate the lidar-measured V_{LOS};
- propagate inputs' uncertainties to the lidar-reconstructed wind characteristics.

2.3. Which Concept to Choose?

The black box calibration concept has the advantages of being fast and relatively easy to implement. Its results include the uncertainties related to the adequacy of the wind model used by the reconstruction algorithm. However, the method has also weaknesses:

1. multiple calibrated reference instruments (with certificates) are necessary to calibrate each of the reconstructed wind characteristics—e.g., cup anemometer for wind speed, vane for wind direction;
2. the assumptions formulated in the reconstruction algorithms may not be completely justified and strongly related to the characteristics of the calibration site—e.g., flow homogeneity in complex terrain;
3. the calibration procedure and setup is specific to the scanning trajectory of the lidar system and to each wind characteristic to calibrate (speed, direction, shear, etc.).
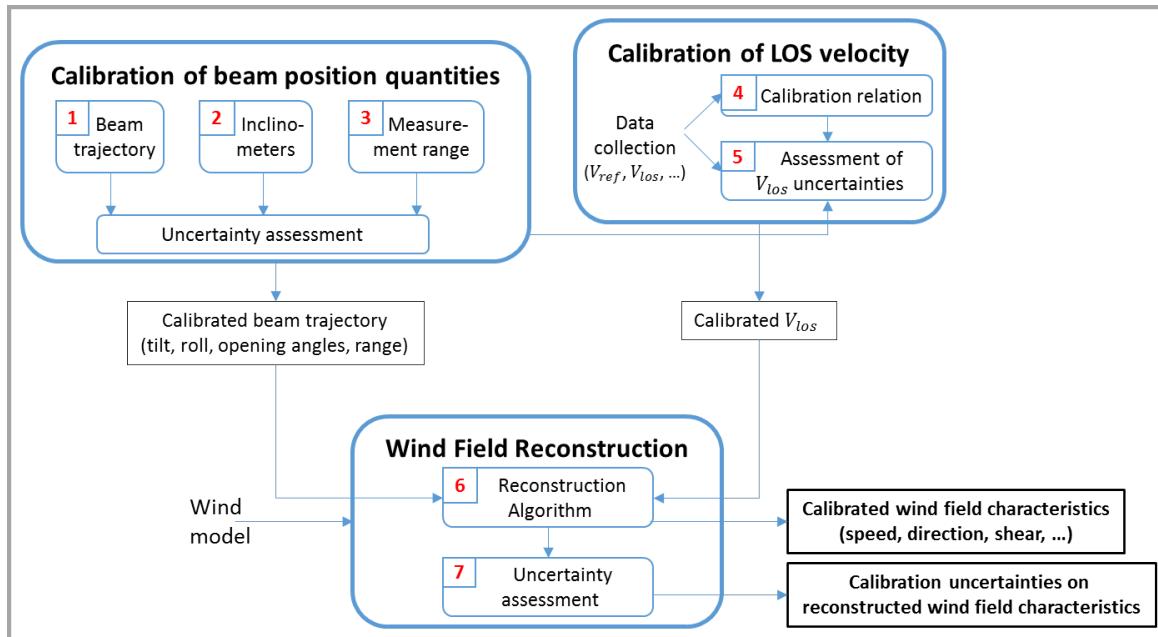
The main advantages of the white box are the calibration of physically existing measurands—as opposed to model estimated wind characteristics—and a lower sensitivity to wind field reconstruction assumptions. The uncertainty evaluation of any reconstructed wind characteristics is theoretically permitted by the white box approach, for example propagating uncertainties with the GUM or Monte-Carlo methods [16].

On the negative side, the calibration duration is longer for multi-beam lidars as formally the V_{LOS} along each LOS—i.e., each optical path—should be calibrated. For a scanning lidar system, only one optical path exists and thus only one LOS calibration is required. Combining the calibration of a single beam with an uncertainty assessment due to deviations between beams may also be considered to reduce the calibration duration. Furthermore, to implement calibration procedures for commercial lidar systems, the reconstruction algorithms will need to be provided (as a minimum, to the calibration laboratory). The veracity of the reconstructed wind characteristics must also be addressed. In other words, the underlying physics behind the reconstruction algorithm must be verified once for each parameter and type of lidar.

Irrespective of the technology and design choices—e.g., continuous wave (CW) vs. pulsed systems; single-beam scanning vs. multi-beam step staring; homodyne vs. heterodyne—Doppler wind lidars all have in common that they measure LOS velocities. Thus, **the path towards a generic calibration procedure of nacelle lidars leads to the white box approach**, which we demonstrate hereafter.

3. White Box Calibration: A Generic Methodology

The white box calibration can essentially be divided into seven steps, as represented in Figure 3.

Figure 3. Schematic of the white box calibration concept for wind lidars.

Knowing accurately where the wind is probed is crucial for the estimation of wind characteristics. Hence, the first three steps relate to the beam's position (see Section 4). Step (1) verifies the geometry of the beam(s)' trajectory. The values of the cone or opening angles are measured and compared to the manufacturer's specification. Step (2) is the inclinometers calibration, needed to correct for the lidar-indicated tilt φ_{ind} and roll ψ_{ind} angles, that are involved in the vertical projection of the reference HWS (Equation (2)). The inclinometers calibration allows uncertainty estimations on φ_{ind} and ψ_{ind}. Steps (1) and (2) should be performed prior to the V_{LOS} measurements as they provide information necessary to the range configuration and data analysis. In step (3) the sensing range—obtained either by ranging or variable focus—is verified. As nacelle lidars measure in a flow having vertical and/or longitudinal gradients, a range error will cause biases.

Steps (4) and (5) are the LOS velocity field measurements and uncertainty assessment, where data from the lidar and reference instrument(s) are collected, the calibration relation obtained, and uncertainties propagated to the lidar-measured V_{LOS} (see Section 5). They constitute the most central part of the white box calibration and can generically be applied to any Doppler wind lidar system.

In steps (6) and (7), wind characteristics are estimated according to the reconstruction algorithms and uncertainties on their outputs assessed (see Section 6). For simple wind models assuming horizontal flow homogeneity, wind characteristics may be derived from an analytical expression, in which case the GUM methodology can be applied (see Section 6.2.2).

Essentially, the genericity of the white box approach lies in the V_{LOS} calibration. Indeed, the procedures to complete steps (1)–(3) are specific to the lidar technology (CW, pulsed, scanning or step-staring, etc.). Steps (6) and (7) depends on the reconstruction algorithm, although the framework for uncertainty assessment may be similar.

4. Calibration/Verification of LOS Positioning Input Quantities

By definition (see [11]), a verification simply consists in checking that a quantity lies within a range close to the expected value, while a calibration additionally corrects the quantity value with the calibration relation and assign uncertainties.

The calibration and/or verification of the beam position input quantities may be performed during field testing or in-house—in which case the lidar manufacturer procedures must be audited

independently. A non-exhaustive list of methodologies to locate the beam includes hard target methods, IR-imaging or the use of IR-sensitive paper.

For the calibration of the 5B and ZDM lidars, the calibration of the inclinometers and verification of the opening or cone angles (steps (1) and (2)) were performed during field testing (Figure 4). As their technology differs, the hard target methods we employed for detecting the beam position were adapted: fixed targets for 5B, moving ones for ZDM. The 3D coordinates of the beam(s)' position were measured with a total station. By placing the lidar in several tilt and roll positions, the inclinometers' readings were compared to the physical tilting and rolling of the beam(s) and a calibration relation was obtained. For 5B, the opening angles can be derived simultaneously to the inclinometers calibration. For ZDM, the geometry parameters are the azimuth position in the scan and the cone angle. The cone angle was derived by fitting the detected beam positions to a circle. To account for potential deviations of the beam trajectory from a circle, an additional uncertainty on the cone angle value may be considered. However, no significant eccentricity was detected during the testing conducted on ZDM. Formally, the accuracy of the azimuth position should also be checked, although we do not expect this to impact significantly the total uncertainties. The detailed procedures and geometrical developments are exemplified in [4,5].

The verification of the sensing range (step (3)) was performed using statistical analysis of the LOS velocity calibration data for 5B, and visual observations of the backscatter levels for ZDM.

Figure 4. Field testing of the 5B (**left**) and ZDM (**right**): inclinometers calibration and beam trajectory verification.

5. LOS Velocity Calibration and Uncertainties

This section provides the methods employed to determine the calibration relation between the lidar-measured V_{LOS} and the reference speed V_{ref} and assess measurement uncertainties. The methods are illustrated through their application to a 5B and a ZDM lidar unit.

For the 5B, the results are presented for LOS0, i.e., the central beam. For ZDM, a $2°$ wide azimuth sector located at the bottom of the scanning trajectory (centered on an azimuth position of $180°$) provides the V_{LOS} measurements to be calibrated. Complete and unit-specific calibration results are reported in [4] for 5B and in [5] for ZDM.

5.1. Reference Quantity

The LOS velocity is calibrated by comparing it to a reference measurand V_{ref} located at the point of focus for a CW lidar and at the centre of the range gate for a pulsed one. V_{ref} is the projection of the wind velocity onto the LOS direction θ_{los}. V_{ref} requires calibrated instruments. A cup and a sonic anemometer—respectively for wind speed and direction—were used to derive V_{ref} as follows:

$$V_{ref} = V_{hor} \cdot \cos\varphi \cdot \cos\underbrace{(\theta - \theta_{los})}_{=\theta_r} \tag{2}$$

where V_{hor} is the HWS, φ is the physical tilt inclination of the lidar beam, θ_r is the relative wind direction, i.e., the difference between the wind and the LOS directions respectively denoted θ and θ_{los}. The definition of V_{ref} is based on time-average measurements of V_{hor}, θ and φ—in this study 10-min periods and vector averages were used. Wind speed and direction variations within the averaging period were therefore assumed to have a negligible impact on instantaneous values of V_{ref}. Equation (2) implicitly neglects the contribution of the vertical component w of the wind vector to the LOS velocity. This approximation is acceptable since for tilt angles $\varphi < 2°$ this contribution is $\sim$3%·w and in flat terrain $w \ll V_{hor}$.

Note that the cup anemometer was preferred for reference wind speed measurements due to the lack of formal uncertainty assessment procedure of sonic-measured wind speed in the current IEC-standards [14].

5.2. Measurement Setup

The measurement setup of a wind lidar field calibration must replicate as closely as possible the conditions in which the lidar measures. Current power performance standards [14] consider 10-min averages of measurements in the 'free stream', typically at 2.5 rotor diameters upstream the turbine. For nacelle lidars, the calibration measurement range should therefore be of the same order, i.e., $\sim$250 m for modern wind turbines.

Depending on the height of the reference instrument(s), maintaining the beam close to the horizontal may demand installing the lidar on a stiff platform at a similar height. With a relatively small mast, the lidar can be positioned on the ground and its beam tilted up. The tilt angle φ should however be limited to avoid measurement errors due to flow inhomogeneities within the inclined probe volume and caused by vertical shear and veer as well as an eventual sensing range error.

The measurement range D_{conf} is defined as the distance between the lidar and the plane orthogonal to the optical centreline (i.e., the symmetry axis of the lidar trajectory, if it exists). D_{conf} must be configured so that:

$$D_{conf} = D \cdot \cos \alpha \qquad (3)$$

where D is the total distance (not the horizontal one) between the lidar and the reference instrument(s), and α the opening angle between the centreline and the LOS to calibrate. D must be accurately measured, for instance using a range-finding theodolite (also called 'total station') or high-resolution GPS.

In the examples of the 5B and ZDM, the calibration was conducted at DTU Wind Energy's test site for large wind turbines, Høvsøre, Denmark. The main site characteristics of Høvsøre are the terrain flatness and a climate featuring high occurrence of strong western winds [17].
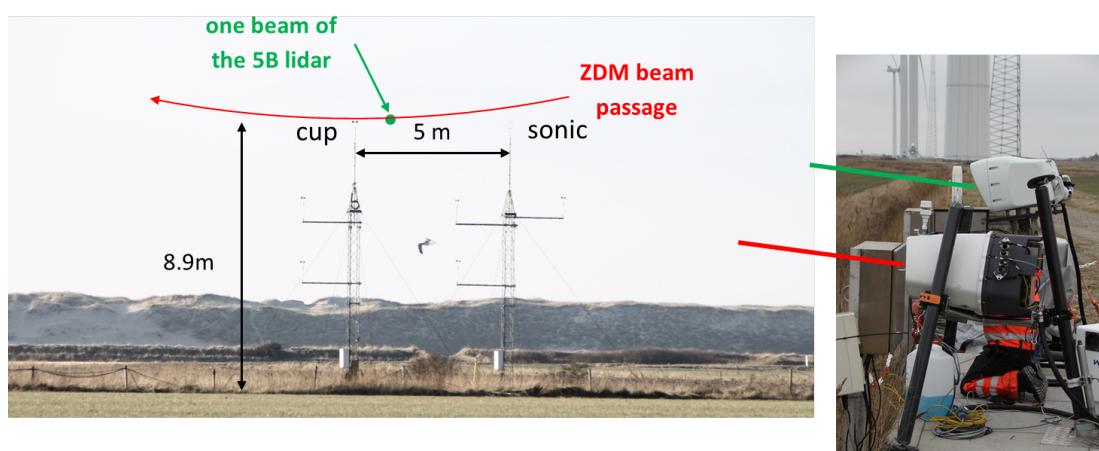
V_{ref} was obtained using a cup (type *Thies First Class Advanced*) and a sonic (type *Gill R3*) anemometer—providing calibrated measurements of V_{hor} and θ respectively. They were top-mounted at $H_{ref} = 8.9$ m agl. (above ground level) on two masts separated by 5 m.

The two nacelle lidars were placed on the ground – on its legs for ZDM, on a special structure for 5B. The distance from the masts was $\sim$260 m. As a result, the physical tilt inclination of the beam from the horizontal was $\varphi \approx 1.6°$—which is different from the reading of the lidar inclinometers. The effective probe lengths at 'half-width half-max' were estimated to 25 m for 5B (constant with the range) and 45 m for ZDM (increase proportionally to the square of the range).

Figure 5 shows the measurement setup in Høvsøre. The beam position was detected using hard target methods and adjusted until its height agl. was the same as the reference instruments. We estimated the standard uncertainty on the beam height to be 10 cm. The lidar beam was positioned close to the reference instrument (Figure 6), with a horizontal separation of $\sim$1–2 m.

Figure 5. Calibration measurement setup at DTU Wind Energy's test site, Høvsøre, Denmark. **Left**: Google Earth image; **Right**: the ZDM and 5B lidars.

Figure 6. Schematic of the beam positions of the 5B (**green**) and ZDM (**red**) lidars at DTU Wind Energy test site, Høvsøre.

5.3. Data Filtering

For the tested 5B and ZDM lidar units, valid 10-min periods were obtained by filtering datasets as follows:

- **Mast**:

  - Cup wind speed $\in [4, 16]$ m·s^{-1}: corresponding to the range of wind speeds for which the cup anemometer is calibrated, in a wind tunnel;
  - Inflow angle (measured by sonic) $\in [-2°, +2°]$: to limit the contamination of V_{LOS} by the vertical wind speed;
  - wind direction θ measured by sonic anemometer $\in \theta_{los} \pm 40°$: except for the 1st step of the LOS direction evaluation process (see Section 5.4), the direction sector is restricted due to the asymmetric geometry of the employed sonic anemometer that can cause flow distortion. Additionally, this corresponds well to normal operational conditions of nacelle lidars since the wind direction relative to the turbine's yaw position is usually $<< 40°$;

- **5B lidar**: carrier-to-noise ratio >-18 dB and LOS availability $>95\%$. LOS availability is the ratio between successful and total attempts to measure V_{LOS}. These two filters ensure the quality and quantity of data measured by the lidar for each 10-min period;
- **ZDM lidar**: LOS availability $\gtrsim 75\%$. The LOS availability is obtained simultaneously to the averaging of high resolution ($\sim$50 Hz) V_{LOS} measurements contained in a specified azimuth sector, that we chose to be $[179°, 181°]$ (i.e., the bottom of the ZDM scanning trajectory). Details on

the employed averaging process can be found in [5]. Note that the lidar was stable enough to ensure the beam was not hitting the cup anemometer.

The filters are only given as an example of those that can reasonably be applied for the LOS velocity calibration. If different lidar systems, units and measurement setups are employed they should be adapted.

5.4. LOS Direction Evaluation

A two-step statistical analysis of the calibration data allows evaluation of the LOS direction θ_{los}. The advantage of the described method is that θ_{los} values are obtained in the frame of the reference sensor used for wind direction measurement.

5.4.1. Fitting the Lidar Response to Wind Direction

θ_{los} is first approximated by fitting the normalised lidar LOS velocity $V_{LOS,norm}$ to a function of the wind direction θ. In this analysis, all wind directions sectors are valid except for site related specifications (e.g., tower shadowing, presence of obstacles, wakes from neighbouring turbines, etc.). The normalised LOS velocity is:
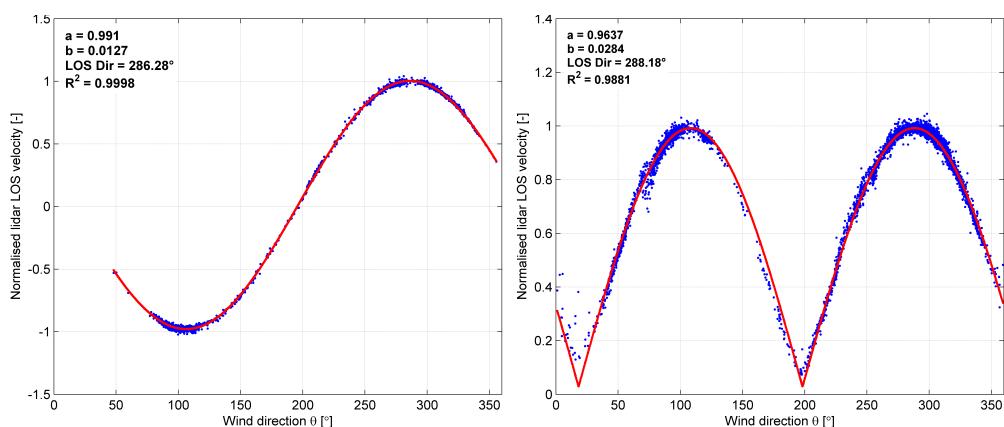
$$V_{LOS,norm} = \frac{V_{LOS}}{V_{hor} \cos \varphi} \tag{4}$$

The fitting function f_{fit} is:

- a cosine wave for a heterodyne lidar (such as 5B): $f_{fit_1} = A_1 \cdot \cos(\theta - \theta_0) + B_1$;
- a rectified cosine wave for a homodyne lidar (such as ZDM): $f_{fit_2} = A_2 \cdot |\cos(\theta - \theta_0)| + B_2$. Homodyne lidars measure only the magnitude of the Doppler shift – not its sign – which translates into positive LOS velocities for any wind direction θ. In such a case, a rectified cosine must be used. The ambiguity in the fitting due to the two distinct solutions for θ_0 is resolved by choosing the value corresponding to the expected bearing of the LOS, e.g., using GPS coordinates;

The least squares fitting yields gain and offset values ideally equal to 1 and 0 respectively. θ_0 is an approximate estimation of θ_{los}.
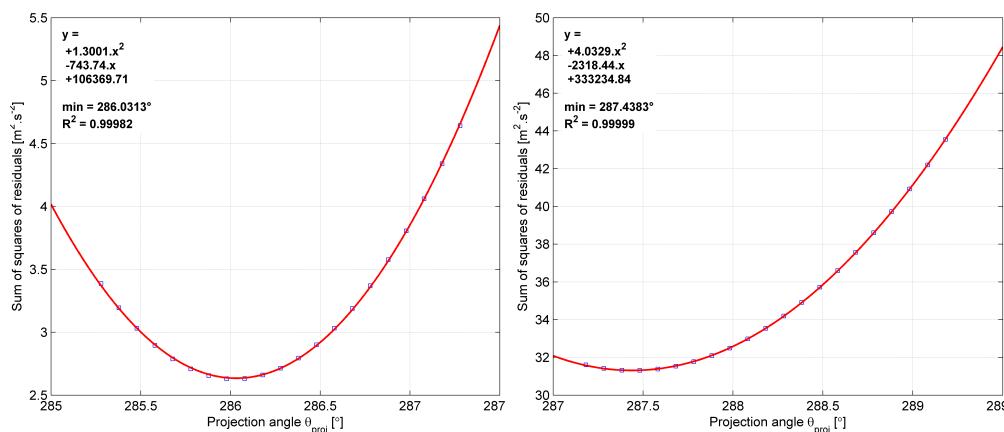
Figure 7 shows the fitting results. The gain and offset values are: 0.99 and 0.01° for 5B; 0.97 and 0.03° for ZDM. The coefficients of determination are both >0.98 thus demonstrating the validity of the method. θ_0 values are 286.28° and 288.18° for the 5B and ZDM lidars respectively.

Figure 7. Lidar response to the wind direction. **Left**: 5B, cosine fitting; **Right**: ZDM, rectified cosine fitting.

5.4.2. Refining the Estimated LOS Direction Using Residuals

A statistical process is further used to refine the estimation of θ_{los}: linear regressions are performed between lidar-measured V_{LOS} and the reference speed V_{hor} projected using angles θ_{proj}—e.g., $\sim$20 values centered around θ_0 with an increment of $0.1°$. Each linear regression yields one Residual Sum of Squares (RSS) value which is then plotted against θ_{proj}. A 2nd order polynomial is fitted to the curve (Figure 8). θ_{los} is taken at the minimum of the parabola. The last step assumes that a minimum of residuals ($\sum \left(V_{LOS} - V_{ref} \right)^2$) is obtained when V_{hor} is projected onto the correct LOS direction. Figure 8 displays the RSS process results.

Figure 8. LOS direction evaluation using the RSS process. **Left**: 5B; **Right**: ZDM.

The final estimations of the LOS direction are: $\theta_{los,5B} = 286.03°$ and $\theta_{los,ZDM} = 287.44°$. We typically observed a difference of $\sim$0.3°–0.7° between the LOS direction θ_{los} provided by the RSS analysis and θ_0 values provided by the cosine fitting. Two plausible explanations affecting the cosine fitting are: lower quality of lidar V_{LOS} measurements for wind directions orthogonal to the LOS; asymmetry of the sonic anemometer's geometry causing biases in measurements outside the preferred direction sector.

The sonic anemometer is aligned to the absolute North, with a mounting uncertainty of $\approx$2°. Using GPS coordinates, θ_{los} was estimated to $\approx$285° and $\approx$286° for 5B and ZDM respectively, which is compatible with the results of the LOS direction evaluation.
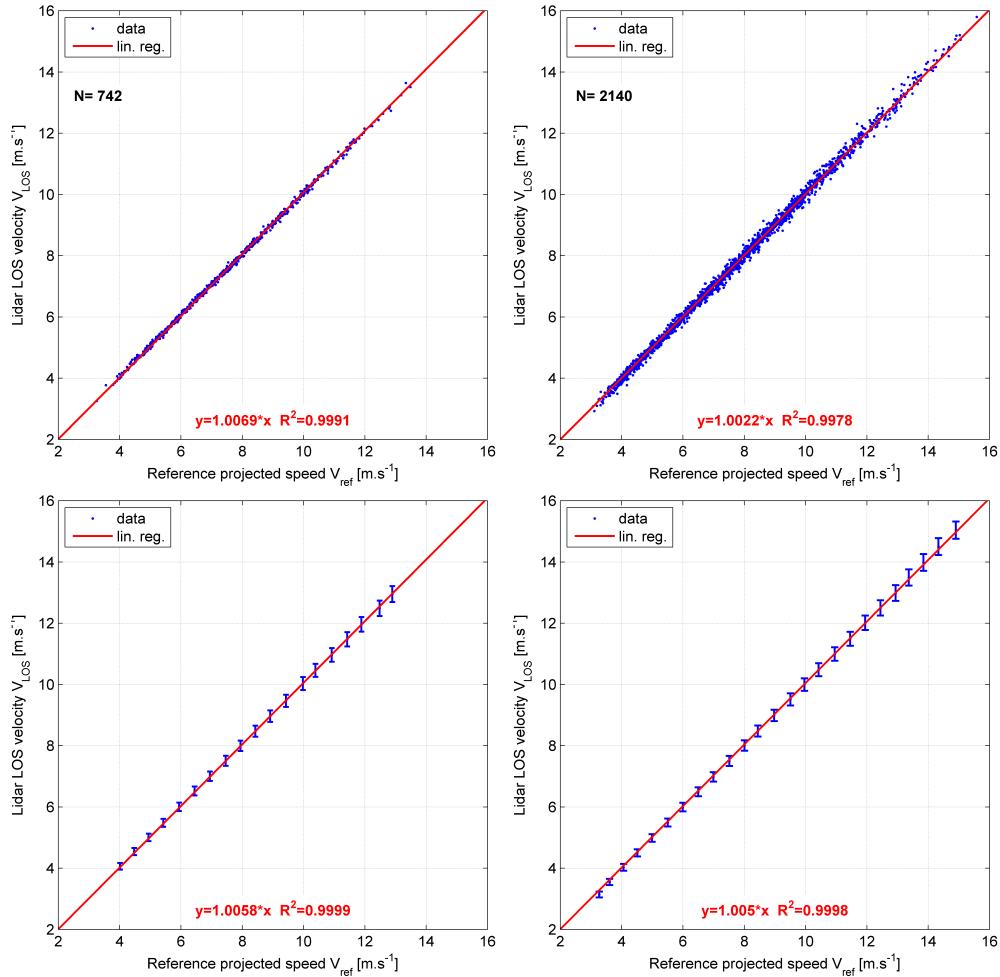
5.5. Calibration Relation

The calibration relation is a linear least squares regression performed on the binned V_{LOS} data. A linear regression is first performed on the valid 10-min data in order to visually identify and investigate outliers, if any. The valid data is then binned based on V_{LOS}. The method of bins disregards the quantity of data in each specific bin, and thus allows the fairest comparison between the lidar-measured V_{LOS} and reference speed V_{ref}. A bin width of 0.5 m·s^{-1} was used, similarly to standard power performance testing. A V_{LOS} bin was considered valid if it contains a minimum of three data points. Completion criteria of the data collection may typically be that all V_{LOS} bins between 4 and 12 m·s^{-1} are valid. Indeed, the measurements are performed in uncontrolled conditions. It can thus be time-consuming to fill in the high wind speed bins.

If the tested lidar performs well, the intercept and slope of the unforced regression are expected to be close to 0 and 1 respectively. **The calibration relation we selected is the linear regression forced to a 0 intercept**. However, both types of linear regression results are valid options for the calibration relation.

Figure 9 shows the calibration relation results and the regression coefficients of the forced linear regressions. Each LOS of 5B has successively been calibrated. For ZDM, we calibrated V_{LOS}

measurements contained in a 2°-wide azimuth sector at the bottom of the beam trajectory. A summary of results is provided in Table 1 (see Section 5.7).

Figure 9. Calibration relation results. **Left column**: 5B; **Right column**: ZDM; **Top row**: 10-min data; **Bottom row**: binned data, including expanded uncertainties in error bars.

The basic filtering applied seems appropriate: no clear outlier is present in the scatter plots of 10-min data. Note that an analysis of the filters significance is provided in the detailed calibration reports of 5B and ZDM (see [4,5]). For both lidars, excellent agreement is obtained between binned V_{LOS} and V_{ref} with consistent gain values showing a difference between 0.5% and 0.9% with the reference (see Table 1). The observed scatter is low: R^2 coefficients are >0.9998.

As the LOS velocity calibration is the most important step of the white box concept, the high quality of the results demonstrate the feasibility of the generic methodology to calibrate profiling nacelle lidars.

5.6. Measurement Uncertainties Assessment Procedure

5.6.1. Definition of uncertainty and the GUM methodology

The VIM [11] defines uncertainty as a:

non-negative parameter characterizing the dispersion of the quantity values being attributed to a measurand, based on the information used.

In essence, the measured quantity value is only an approximation of the unknowable true value, i.e., only a best estimate. The uncertainty of a measured quantity value defines the interval centered on the best estimate and within which the true value lies with a certain probability.

In this paper, V_{LOS} uncertainties are assessed using the GUM methodology [12]. The main steps are summarised hereafter:

1. define the measurement model: $y = f(x_1, \ldots, x_n)$ where y is the best estimate and $x_1, \ldots, x_n$ are the input quantities;
2. list the input quantities and determine their uncertainties $u_{x_1}, \ldots, u_{x_n}$;
3. evaluate covariances between the uncertainties of the input quantities;
4. calculate the measured value y;
5. combine the uncertainties on the input quantities using the law of propagation of uncertainties to obtain $u_{c,y}$;
6. derive and report the expanded uncertainty $U_y = k \cdot u_{c,y}$ where k is the coverage factor (see definition 2.38 in [11]).

Note: the notations employed here for uncertainties of an arbitrary quantity x are: u_x standard uncertainty (i.e., coverage factor $k = 1$); $u_{c,x}$ combined uncertainty; U_x expanded uncertainty.

The GUM methodology relies on the law of propagation of uncertainties (see Section 5.2.2 in [12]) given by :

$$u_{c,y} = \sqrt{\sum_{i=1}^{N} \sum_{j=1}^{N} \frac{\partial f}{\partial x_i} \frac{\partial f}{\partial x_j} u_{x_i} u_{x_j} r_{ij}} \tag{5}$$

where x_i and y are respectively the input quantities and output of the measurement model f, r_{ij} is the correlation coefficient between the uncertainty distributions of x_i and x_j with $i, j \in [1, N]$. Equation (5) is the most general form of the law of propagation of uncertainties. For uncorrelated input quantities, in other words independent variables (see Section 5.1.2 in [12]), $r_{ij} = 0$ when $i \neq j$ and Equation (5) is simplified to:

$$u_{c,y} = \sqrt{\sum_{i=1}^{N} \left(\frac{\partial f}{\partial x_i} \right)^2 u_{x_i}^2} \tag{6}$$

5.6.2. Applying the GUM to the Calibration of V_{LOS}

The GUM is applied to the calibration relation between the lidar-measured V_{LOS} and V_{ref}. The measurement model defining the estimated measurand is:

$$y = a \cdot V_{ref} \tag{7}$$

where a is the gain of the forced linear regression on the binned calibration data. Using the law of propagation of uncertainties for uncorrelated input quantities (Equation (6)), we obtain:

$$u_{c,y} = \sqrt{a^2 u_{c,V_{ref}}^2 + V_{ref}^2 u_a^2} \tag{8}$$

The uncertainty u_a is taken as the half-width of the 68% confidence interval (CI) on a (equivalent to a coverage factor $k = 1$ for normally distributed uncertainties). The method to estimate u_a is based on QR-decomposition and T-tests. The order of magnitude of u_a is $10^{-3}[-]$. For LOS 0 of 5B, $u_{a,5B,los_0} = 7.1 \times 10^{-4}$. For ZDM, $u_{a,ZDM} = 1.1 \times 10^{-3}$. Considering this measurement model,

once measuring stand-alone, the best estimate of the lidar-measured V_{LOS} is defined by the reciprocal of the calibration relation:

$$V_{LOS,be} = \frac{V_{LOS}}{a} \tag{9}$$

and its corresponding calibration uncertainty is $u_{c,y}$.

5.6.3. Combined Uncertainty on V_{ref}

In this study, classic anemometry is used to provide V_{ref} (Equation (2)). $u_{c,V_{ref}}$ is derived by combining uncertainties from the reference instruments with the calibration process uncertainties. For the sake of simplicity, and as φ, V_{hor}, θ and θ_{los} are measurements taken by independent systems, their uncertainties can reasonably be assumed uncorrelated. The law of propagation of uncertainties gives:

$$u_{c,V_{ref}} = \sqrt{\left(\frac{\partial V_{ref}}{\partial V_{hor}} \cdot u_{c,V_{hor}} \right)^2 + \left(\frac{\partial V_{ref}}{\partial \varphi} \cdot u_{\varphi} \right)^2 + \left(\frac{\partial V_{ref}}{\partial \theta_r} \cdot u_{c,\theta_r} \right)^2} \tag{10}$$

where $\theta_r = \theta - \theta_{los}$ is the relative wind direction. Based on Equation (2), the partial derivatives are computed for each valid 10-min period:

$$\begin{cases} \frac{\partial V_{ref}}{\partial V_{hor}} = \cos \varphi \cos \theta_r \\ \frac{\partial V_{ref}}{\partial \varphi} = -V_{hor} \sin \varphi \cos \theta_r \\ \frac{\partial V_{ref}}{\partial \theta_r} = -V_{hor} \sin \theta_r \cos \varphi \end{cases} \tag{11}$$

At this stage of the uncertainty assessment procedure, only the values of $u_{c,V_{hor}}$, u_{φ} and u_{c,θ_r} are missing. The uncertainty budget (Section 5.6.4) provides their estimation. Note that angle uncertainties must be expressed in radians when computing the combined uncertainty.

5.6.4. Uncertainty Sources and Budget

The uncertainty evaluation of the cup-measured reference speed V_{hor} follows the IEC-61400-12-1 standard (Annex E in [14]). It should be mentioned that most of the numeric values used in this standard are empirical and somewhat arbitrary. For the LOS velocity calibration procedure, the HWS uncertainty sources are:

(i) **Wind tunnel calibration uncertainty**:

$$u_{cal} = \sqrt{u_{cal,1}^2 + \left(\frac{0.01}{\sqrt{3}} V_{hor} \right)^2} \tag{12}$$

where $u_{cal,1}$ is the uncertainty specified by the calibration certificate for a coverage factor $k = 1$. We used $u_{cal,1} \approx 0.025 \text{ m} \cdot \text{s}^{-1}$. The 2nd term is due to the variability of cup anemometers calibration results for *Measnet* accredited wind tunnels. *Measnet* requires the tunnels to be within $\pm 1\%$ of each other. Hence a 1% uncertainty is added with an assumed rectangular—or uniform—distribution of uncertainty yielding the $1/\sqrt{3}$ factor.

(ii) **Operational—also called classification—uncertainty**:

$$u_{ope} = \frac{k_{class}}{\sqrt{3}} \cdot (0.05 + 0.005 V_{hor}) \tag{13}$$

where k_{class} is the anemometer's classification number characterising the systematic deviations due to environmental conditions, e.g., angular response, turbulence, temperature (influence on

bearing friction), etc. The cup anemometer used in this study is of type *'Thies First Class Advanced'* which has a class of 0.9A ($k_{class} = 0.9$).

(iii) **Mounting uncertainty**:

$$u_{mast} = 0.5\% \cdot V_{hor} \tag{14}$$

related to the mounting of the sensor on the mast. The 0.5 % uncertainty is the default value for top-mounted instruments suggested in the revision of the IEC 61400-12-1.

The only source of **wind direction uncertainty** from the sonic anemometer is the calibration. Indeed, the LOS direction is evaluated in the frame of reference of the wind direction sensor (see Section 5.4). The North mark and boom orientation uncertainties are thus irrelevant. At $k = 1$, the calibration certificates specify a wind direction uncertainty of

$$u_\theta = 0.4° \tag{15}$$

Uncertainty sources in the calibration measurement process are:

(i) LOS direction uncertainty, related to the statistical evaluation of θ_{los} (Section 5.4) and roughly estimated to:

$$u_{\theta_{los}} = 0.1° \tag{16}$$

(ii) Uncertainty of physical inclination angle characterising the uncertainty of the angle used in the vertical projection of the HWS in (Equation (2)) and estimated via the inclinometers' calibration (see [4,5]) to:

$$u_\varphi = 0.05° \tag{17}$$

(iii) Vertical beam positioning uncertainty: characterises how close to the reference instruments height the beam is positioned. Here, modelling the vertical shear profile with the power law, using a shear exponent $\alpha_{exp} = 0.2$, a height uncertainty $u_H = 10$ cm at $H_{ref} = 8.9$ m, the wind speed uncertainty due to the height error is:

$$u_{pos} = \alpha_{exp} \cdot \frac{u_H}{H_{ref}} \cdot V_{hor} \approx 0.23\% \cdot V_{hor} \tag{18}$$

(iv) Inclined beam and range uncertainty: practically, the inclined beam implies that the laser light travels, within the probe volume, through a range of heights. The lidar thus senses different wind speeds if there is a wind shear. Additionally, the range uncertainty along the LOS moves the probe volume's center slightly away from the reference instruments' height. A model of this uncertainty can be found in Annex A of [18]. Configuring this model with the 5B and ZDM lidars setup in Høvsøre and a conservative 5 m range uncertainty, we obtained respectively:

$$\begin{cases} u_{inc,5B} = 0.052\% \cdot V_{hor} \\ u_{inc,ZDM} = 0.104\% \cdot V_{hor} \end{cases} \tag{19}$$

(v) Spatial separation uncertainty: the spatial separation between the two reference sensors infers an uncertainty whose magnitude increases with the separation distance. In our case, the two masts are 5 m apart and the terrain is flat. The spatial separation effects can reasonably be neglected.

The combined uncertainty components in Equation (10) are finally computed as follows:

$$\begin{cases} u_{c,V_{hor}} = \sqrt{u_{cal}^2 + u_{ope}^2 + u_{mast}^2 + u_{pos}^2 + u_{inc}^2} \\ u_{c,\theta_r} = \sqrt{u_\theta^2 + u_{\theta_{los}}^2} \end{cases} \tag{20}$$

5.6.5. Expanded V_{LOS} Uncertainties

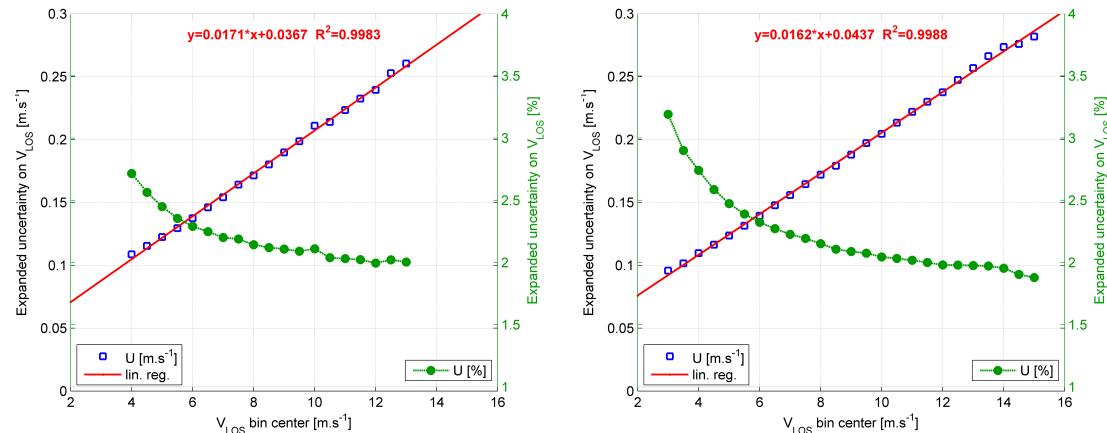Given a coverage factor k, the expanded LOS velocity uncertainty is:

$$U_{c,y} = k \cdot u_{c,y} \tag{21}$$

Classically, the value of $k = 2$ is chosen in which case $U_{c,y}$ corresponds to the half-width of a 95% CI for a normal probability distribution. If $k = 1$, it corresponds to a 68% CI; if $k = 3$, to a 99% CI.

The combined and expanded uncertainty values depend on the encountered wind conditions (speed, direction, tilting, etc.). Thus, they are computed for each valid 10-min period. They are then averaged in each V_{LOS} bin and may be reported in the form of a table (see [4,5]).

The expanded V_{LOS} measurement uncertainties of 5B and ZDM averaged per bin are displayed in Figure 10. They vary linearly with the LOS velocity ($R^2 > 0.99$). High wind speed bins for the calibration of LOS0 of the 5B lidar do not feature enough data points and are invalid for $V_{LOS} > 13 \text{ m·s}^{-1}$. However, the linearity of the uncertainties suggests that extrapolation of the uncertainties to the invalid bins is reasonable.

With a coverage factor $k = 2$, the expanded uncertainties vary from $\approx$3.2% at 3 m·s^{-1} to $\approx$1.9% at 16 m·s^{-1}, as shown in Figure 10's right axis. The uncertainties results obtained show insignificant deviations between ZDM and all LOS of 5B.

Figure 10. Expanded LOS velocity measurement uncertainties in m·s^{-1} and in % of V_{LOS}. **Left**: 5B; **Right**: ZDM.

5.7. Summary of Calibration Results

The calibration results obtained for the 5B and ZDM lidars are summarised in Table 1.

Table 1. Summary of LOS velocity calibration results.

Lidar	LOS	Calibration Relation				Expanded Uncertainties ($k = 2$)		
		θ_{los}	a	R^2	$Npts$	U (m·s^{-1})	U at 4 m·s^{-1}	U at 16 m·s^{-1}
5B	LOS 0	286.03°	1.0058	0.9999	742	$0.0171 \cdot V_{LOS} + 0.0367$	2.72%	1.94%
	LOS 1	285.99°	1.0072	0.9999	502	$0.0156 \cdot V_{LOS} + 0.0460$	2.73%	1.84%
	LOS 2	285.99°	1.0084	1.0000	1087	$0.0157 \cdot V_{LOS} + 0.0449$	2.73%	1.85%
	LOS 3	286.06°	1.0090	0.9999	446	$0.0152 \cdot V_{LOS} + 0.0476$	2.73%	1.82%
	LOS 4	285.99°	1.0059	1.0000	1508	$0.0155 \cdot V_{LOS} + 0.0457$	2.68%	1.84%
ZDM	179°–181° azimuth	287.44°	1.0050	0.9998	2140	$0.0162 \cdot V_{LOS} + 0.0437$	2.75%	1.89%

6. Uncertainties of Reconstructed Wind Characteristics

In this section, the reconstruction case of a two-beam nacelle lidar system is used to demonstrate how, as facilitated by the white box methodology, uncertainties on multiple wind characteristics can be estimated. The propagation of calibration uncertainties through the reconstruction algorithm does not account for the flow model inadequacy. The wind model should be validated separately, and the uncertainty due to its inadequacy assessed.

6.1. Wind Field Reconstruction Techniques

To reconstruct wind characteristics from single Doppler wind lidar data, hypotheses on the flow field must be made, i.e., a flow model is assumed.

Examples of spatial assumptions that may be employed in wind field reconstruction (WFR) are: horizontal homogeneity (e.g., VAD techniques classically used by ground-based lidars); two- or three-dimensional wind vector; vertical and/or longitudinal shear profile (linear, power law, log-law, etc.). These assumptions are sufficient for static WFR (see [8], suitable for power performance applications), which disregards the propagation of the wind field over time. In the dynamic case (see [19,20], suitable for turbine control applications) flow models may additionally assume specific velocity and turbulence field structures (coherence) and Taylor's frozen turbulence hypothesis.

Once the flow model is defined, a least squares problem can be formulated: lidar measurements may be fitted to the model by projecting wind characteristics onto multiple LOS, thus minimising errors between 'simulated' and measured LOS velocities.

When the least squares problem is linear (such as in certain cases of flow homogeneity), analytical expressions of wind characteristics can be derived by matrix inversion [8].

The usable methods to propagate uncertainties on V_{LOS} and other inputs to wind characteristics depend on the complexity of the WFR. Numerical techniques such as Monte-Carlo, bootstrap or Polynomial Chaos Expansion may be implemented. Although they might be computationally expensive, they are particularly relevant for non-linear flow models where advanced WFR fitting techniques are employed. The aforementioned uncertainty propagation methods are additionally appropriate to handle correlation between uncertainty distributions. Details on advanced WFR techniques and the corresponding uncertainty propagation methods are outside the scope of this paper.
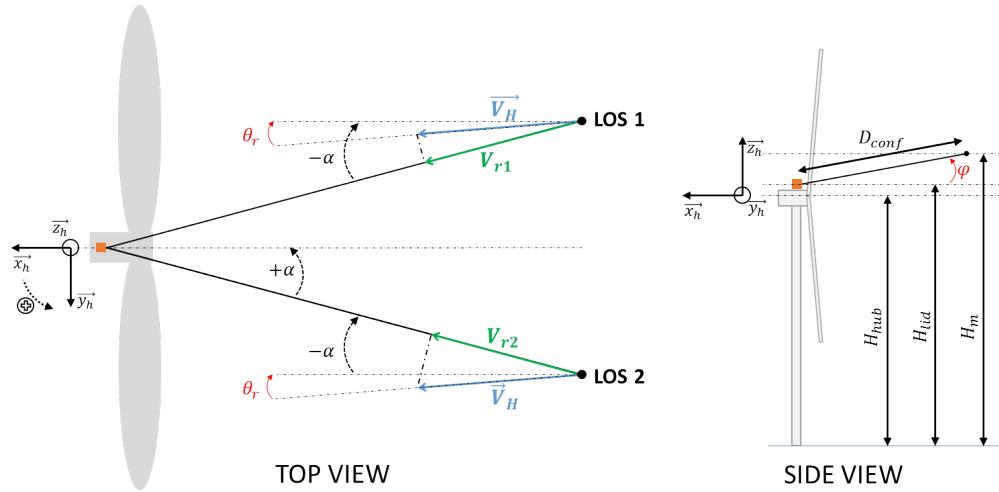
For the two-beam lidar case hereafter, we chose to apply the GUM methodology as simple analytical expressions of wind characteristics are available.

6.2. Example for a Two-Beam Nacelle Lidar

6.2.1. Reconstruction Algorithm

We here use a simple reconstruction algorithm applied to a two-beam nacelle lidar, see Figure 11. Although the flow model described hereafter is expected to be strongly inadequate for multiple-beam profiling nacelle lidars, the example corresponds to the technique employed by the first generation of

commercial systems—such as the two-beam *Avent Wind Iris* and pair-derived wind characteristics that can be extracted from the *ZephIR Dual Mode* lidar—hence its relevance.

Figure 11. Two-beam nacelle lidar schematics for wind field reconstruction.

At one specific range, the hypotheses of the flow model are:

(1) two-dimensional wind vector: the vertical component V_z is 0, downstream and transverse components are denoted V_x and V_y respectively;

(2) horizontal flow homogeneity: V_x and V_y are independent of the y_h coordinates (see Figure 11) of the beams position;

(3) the probe volume averaging is neglected: time-averaged lidar V_{LOS} are considered as point-like quantities;

(4) the lidar roll inclination is $0°$: both beams sense winds at the same height.

The LOS velocities are given by:

$$\begin{cases} V_{r1} = V_H \cos\varphi \cos(\alpha + \theta_r) \\ V_{r2} = V_H \cos\varphi \cos(\alpha - \theta_r) \end{cases} \tag{22}$$

where V_H is the horizontal wind speed, θ_r the wind direction relative to the turbine's yaw position, α the lidar half-opening angle, φ the lidar tilt inclination. The wind vector components are then:

$$\begin{cases} V_x = V_H \cos(\theta_r) \\ V_y = V_H \sin(\theta_r) \end{cases} \equiv \begin{cases} V_x = \frac{V_{r1}+V_{r2}}{2\cos\varphi\cos\alpha} \\ V_y = \frac{-V_{r1}+V_{r2}}{2\cos\varphi\sin\alpha} \end{cases} \tag{23}$$

Finally, the wind speed and relative direction are derived as follows:

$$\begin{cases} V_H = \sqrt{V_x^2 + V_y^2} \\ \theta_r = \mathrm{atan}\left(\frac{V_y}{V_x}\right) \end{cases} \tag{24}$$

In normal operations, the turbine yaws according to the wind direction, θ_r is expected to be close to 0. Hence, for simplicity, we used the arctangent function (atan) instead of its four-quadrant extension (atan2).

u_{θ_r} (Equation (27)) is only the calibration uncertainty of the relative direction. Practically, the alignment of the lidar to the nacelle centreline is an additional source of uncertainty—its magnitude will depend on the mounting procedure – that must be accounted for by quadratically adding it to u_{θ_r}.

In real-world applications, the lidar tilt will follow closely the nacelle's motion. The two reconstructed wind characteristics are thus valid at the H_m height agl:

$$H_m = H_{lid} + D_{conf} \sin(\varphi) \tag{25}$$

where H_{lid} is the lidar height agl. and D_{conf} the configured measurement range. In the case where the aim is to estimate the wind speed at hub height, as it usually is in power performance testing, a correction of the wind speed reconstructed at H_m should be made, if possible. The issue of nacelle lidars probing the wind at a single height implies an extra uncertainty, characterising the wind speed uncertainty caused by the motion of the turbine's nacelle.

6.2.2. Propagating Uncertainties with the GUM

Applying the law of propagation of uncertainties to the expressions of V_x, V_y (Equation (23)), we obtain:

$$\begin{cases} u_{V_x}^2 = \left(\frac{1}{2\cos\varphi\cos\alpha}\right)^2 \cdot \left(u_1^2 + u_2^2 + 2r_{1,2}u_1u_2\right) + V_x^2\left(\tan^2\varphi \cdot u_\varphi^2 + \tan^2\alpha \cdot u_\alpha^2\right) \\ u_{V_y}^2 = \left(\frac{1}{2\cos\varphi\sin\alpha}\right)^2 \cdot \left(u_1^2 + u_2^2 - 2r_{1,2}u_1u_2\right) + V_y^2\left(\tan^2\varphi \cdot u_\varphi^2 + \frac{u_\alpha^2}{\tan^2\alpha}\right) \end{cases} \tag{26}$$

where $r_{1,2}$ is the correlation coefficient between the uncertainties u_1, u_2 on V_{r1} and V_{r2}. We implicitly assumed that the uncertainties u_φ and u_α are correlated neither with u_1, u_2 nor between each other. Then, the law of propagation is applied to Equation (24) to obtain the wind speed and relative direction uncertainties, respectively denoted u_{V_H} and u_{θ_r}:

$$\begin{cases} u_{V_H}^2 = \frac{1}{V_H^2} \cdot \left(V_x^2 u_{V_x}^2 + V_y^2 u_{V_y}^2 + 2r_{xy}V_xV_yu_{V_x}u_{V_y}\right) \\ u_{\theta_r}^2 = \frac{1}{V_H^4} \cdot \left(V_y^2 u_{V_x}^2 + V_x^2 u_{V_y}^2 - 2r_{xy}V_xV_yu_{V_x}u_{V_y}\right) \end{cases} \tag{27}$$

6.2.3. Uncertainty Budget, Results and Scale Analysis

In this paragraph, LOS velocities V_{r1} and V_{r2} are 'simulated' according to Equation (22). All results are obtained with a half-opening angle $\alpha = 15°$—typical of commercial systems—and a tilt $\varphi = -1°$. At a coverage factor $k = 1$, the uncertainty budget is:
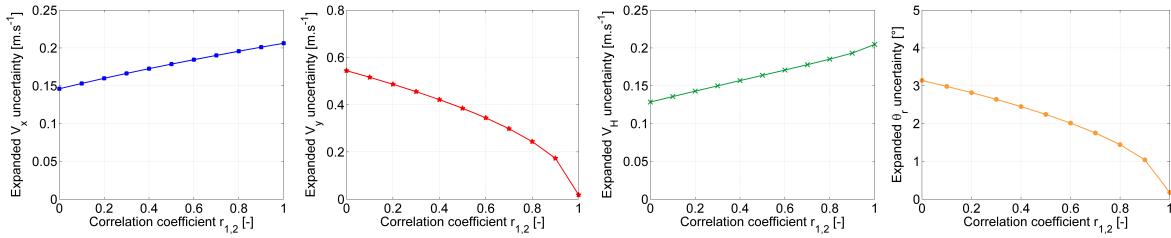
(i) LOS velocity: taking advantage of the previously observed linearity (see Section 5.6.5), the LOS velocity uncertainty of beam i is estimated to $u_i = m \cdot V_{ri} + n$ where $m = 0.008$ and $n = 0.0225$. We here obtained m and n by approximating the gain and offset value of the expanded uncertainty linear relation (see Table 1) and dividing it by the coverage factor;

(ii) Tilt inclination: $u_\varphi = 0.05°$ as prescribed by the inclinometers calibration;

(iii) Opening angle: from the geometry verification, we estimate $u_\alpha = 0.1°$.

In the GUM methodology, the correlation between uncertainty components may have a large impact on the combined uncertainty. The variability of uncertainty results depending on the correlation between u_1 and u_2 is shown in Figure 12. In the full correlation case, both expanded uncertainties U_{V_x} and U_{V_H} are ~50% higher than in the uncorrelated one. The effect is even more critical for U_{V_y} and U_{θ_r}: the calibration uncertainty is almost zero for $r_{1,2} = 1$. Note that an extra uncertainty quantifying the wind model inadequacy should be added to the calibration uncertainty.
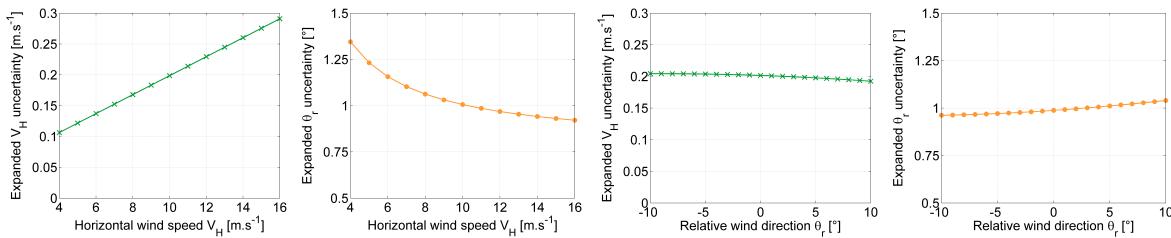
In practice, the LOS velocity calibration will probably be performed for both beams at the same site, with the same reference instruments. Moreover, the reference instruments contribute for >90% to the total V_{LOS} uncertainty (7.1). u_1 and u_2 are most likely highly and positively correlated. In the next paragraphs, we arbitrarily choose $r_{1,2} = 0.9$ and $r_{xy} = 0.2$, later shown to be negligible.

Figure 13 displays expanded uncertainties as a function of wind speed (with $\theta_r = 5°$) and direction (with $V_H = 10$ m·s^{-1}). U_{V_H} varies linearly with V_H and is approximately of same magnitude as $U_{V_{LOS}}$.

The wind direction uncertainty U_{θ_r} decreases with the wind speed. The relative wind direction has little impact on U_{V_H} and U_{θ_r}, as long as it stays within a reasonable range.

Figure 12. Expanded uncertainties U_{V_x}, U_{V_y}, U_{V_H} and U_{θ_r} as a function of correlation coefficient $r_{1,2}$ ($V_H = 10$ m·s^{-1}, $\theta_r = 5°$, $r_{xy} = 0.2$).

Figure 13. Expanded uncertainties U_{V_H} and U_{θ_r} as a function of V_H and θ_r ($r_{1,2} = 0.9$ and $r_{xy} = 0.2$).

Seeking to identify which terms of Equations (26) and (27) are dominant, a scale analysis is conducted (Table 2) with $V_H \sim 10$ m·s^{-1} and $\theta_r \sim 10^{-1}$ rad $\approx 5°$.

Table 2. Scale analysis of uncertainty components contributing to uncertainties on V_x V_y, V_H and θ_r.

Combined Uncertainty	Uncertainty Term and Order of Magnitude				
$u_{V_x}^2$ in $\left[\text{m}^2 \cdot \text{s}^{-2}\right]$	$\dfrac{u_1^2}{(2\cos\varphi\cos\alpha)^2}$	$\dfrac{u_2^2}{(2\cos\varphi\cos\alpha)^2}$	$\dfrac{2r_{1,2}u_1u_2}{(2\cos\varphi\cos\alpha)^2}$	$V_x^2 \tan^2\varphi \cdot u_\varphi^2$	$V_x^2 \tan^2\alpha \cdot u_\alpha^2$
	10^{-3}	10^{-3}	10^{-3}	10^{-7}	10^{-5}
$u_{V_y}^2$ in $\left[\text{m}^2 \cdot \text{s}^{-2}\right]$	$\dfrac{u_1^2}{(2\cos\varphi\sin\alpha)^2}$	$\dfrac{u_2^2}{(2\cos\varphi\sin\alpha)^2}$	$\dfrac{-2r_{1,2}u_1u_2}{(2\cos\varphi\sin\alpha)^2}$	$V_y^2 \tan^2\varphi \cdot u_\varphi^2$	$\dfrac{V_y^2 u_\alpha^2}{\tan^2\alpha}$
	10^{-1}	10^{-1}	-10^{-1}	10^{-9}	10^{-4}
$u_{V_H}^2$ in $\left[\text{m}^2 \cdot \text{s}^{-2}\right]$	$\dfrac{V_x^2 u_{V_x}^2}{V_H^2}$	$\dfrac{V_y^2 u_{V_y}^2}{V_H^2}$	$\dfrac{2r_{xy}V_x V_y u_{V_x} u_{V_y}}{V_H^2}$		
	10^{-2}	10^{-4}	10^{-3}		
$u_{\theta_r}^2$ in $\left[\text{rad}^2\right]$	$\dfrac{V_y^2 u_{V_x}^2}{V_H^4}$	$\dfrac{V_x^2 u_{V_y}^2}{V_H^4}$	$\dfrac{-2r_{xy}V_x V_y u_{V_x} u_{V_y}}{V_H^4}$		
	10^{-6}	10^{-4}	10^{-6}		

Concerning u_{V_x} and u_{V_y}, the tilt and opening angle uncertainties are negligible, irrespective of $r_{1,2}$. Uncertainties u_{V_H} and u_{θ_r} are governed respectively by the uncertainty on the downstream and transverse component. The correlation term can be neglected irrespective of the value of r_{xy}. Equations (26) and (27) can thus be approximated by:
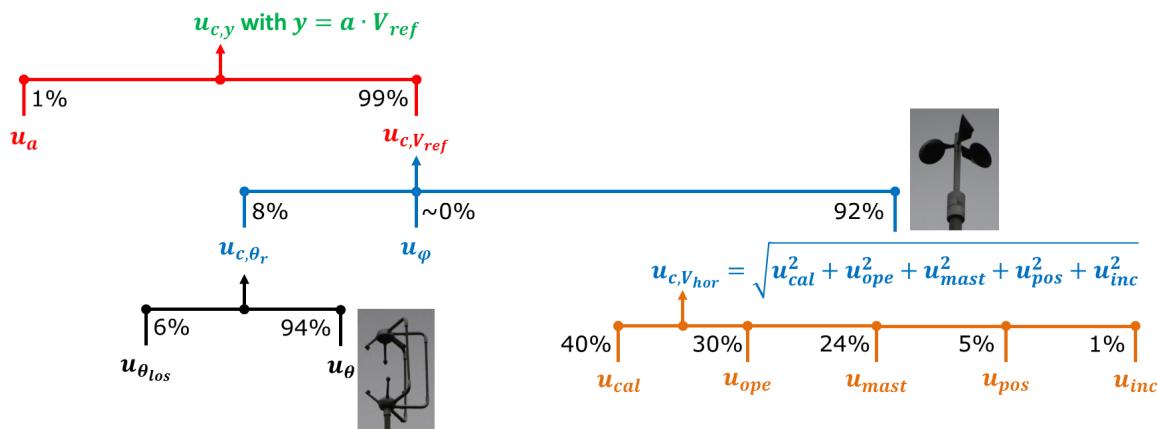
$$
\begin{cases}
u_{V_x}^2 \approx \dfrac{u_1^2 + u_2^2 + 2r_{1,2}u_1u_2}{(2\cos\varphi\cos\alpha)^2} \\
u_{V_y}^2 \approx \dfrac{u_1^2 + u_2^2 - 2r_{1,2}u_1u_2}{(2\cos\varphi\sin\alpha)^2}
\end{cases}
\quad \text{and} \quad
\begin{cases}
u_{V_H}^2 \approx \dfrac{V_x^2 u_{V_x}^2}{V_H^2} \\
u_{\theta_r}^2 \approx \dfrac{V_x^2 u_{V_y}^2}{V_H^4}
\end{cases}
\tag{28}
$$

7. Discussion

7.1. On Lidar V_{LOS} Uncertainties

An analysis of the measurement uncertainty results is performed in order to identify the prevailing uncertainty sources. Figure 14 illustrates the uncertainty assessment procedure in the form of a tree structure. From bottom to top, the approximate contribution of each uncertainty source to the next level of combined uncertainty is given. For example, the contribution of u_{mast} to $u_{c,V_{hor}}$ is computed as $u_{mast}^2/u_{c,V_{hor}}^2$. This analysis demonstrates that:

(1)   the uncertainty of the reference quantity $u_{c,V_{ref}}$ accounts for 99% of the combined LOS velocity uncertainty $u_{c,y}$;

(2)   >90% of the reference speed uncertainty $u_{c,V_{ref}}$ is related to the combined reference HWS uncertainty $u_{c,V_{hor}}$;

(3)   ~94% of $u_{c,V_{hor}}$ is due to the cup anemometer's calibration, operational and mast uncertainties. The LOS velocity calibration process accounts only for the remaining 6% with u_{inc} and u_{pos}.

Figure 14. The 'tree' structure of the uncertainty assessment methodology including relative contributions of individual uncertainty sources.

Consequently, a **great majority of the total uncertainty on the LOS velocity is due to the calibration, operational and mast-mounting uncertainty components on the reference quantity**.

This conclusion emphasises the need to improve the cup anemometer uncertainty assessment methodology. In particular, the spread of 1% between *Measnet* accredited wind tunnels is unacceptably large: wind speed measurements from a cup anemometer should not be significantly dependent on the wind tunnel in which it is calibrated. Additionally, measurement errors due to the cup anemometers' sensitivities—to temperature, turbulence intensity, inflow angles, etc.—is incorporated through the classification uncertainty. If such systematic errors can be estimated, they are biases (see definition in VIM, [11]) and should be corrected for instead of considering them as an extra uncertainty.

Currently, improvements in the generic calibration procedure cannot be easily identified since the uncertainty components related to the calibration process account for a negligible proportion of the total LOS velocity uncertainty.

The main goal of this study is to propose and demonstrate a generic calibration procedure in order to make lidar measurements traceable to the International System of Units. Although a single sonic anemometer may conveniently replace the dual-instrument setup, no procedure to assess sonic anemometers' measurement uncertainties is given in the IEC 61400-12-1:2005 norm (but will be in the next revision, see [14]). Thus, the constrain was to use a cup anemometer for the HWS reference instrument. In addition, the wind industry shows a conservative attitude towards wind measurements: for decades, only cup anemometers had been considered.

Alternatively, in the future, lidar-to-lidar calibrations may be performed, using a calibrated lidar as a reference. The principles of the 'white box' calibration will remain valid—replacing V_{ref} by the reference lidar V_{LOS} measurements and directly using uncertainties provided by the calibration certificate. Only slight adjustments of the procedure are anticipated. Lidar-to-lidar calibrations would reduce the calibration duration, however not the uncertainty.

7.2. On Repeatability in Field Measurements

One particularity of field measurements in wind energy is that atmospheric conditions cannot be controlled. Therefore, repeatability does not formally exist. Repeatable conditions could be defined by grouping data according to wind speed, turbulence intensity, temperature, aerosols concentration, thermal stability, etc. Obtaining sufficiently large calibration datasets under repeatable conditions would require years of measurement data and is consequently not reasonably feasible. Thus, LOS velocity measurement uncertainties cannot be assessed using only statistical methods (of 'type A', [11]). Studies of long-term measurement datasets would provide valuable information on the statistical uncertainties of lidar measurements, both at the LOS velocity and reconstructed parameter level. Such studies may even allow to obtain a 'golden' calibrated lidar that could then be used as a reference for other lidars calibration. However, to the author's knowledge, no such studies exist or are ongoing at the time of writing.

7.3. On Limitations of the Application of the White Box

The white box calibration examples demonstrated in this paper feature some limitations—mostly practical—that must be mentioned.

First, the uncertainty components from the reference instruments prevail, emphasizing the need for improving calibration procedures for cup anemometers. Second, the measurement setup is not ideal as measuring at low height above the ground implies high turbulence intensity, which can affect both the reference and lidar measurements, or potential aerosol gradients. On the other hand, a tall mast would require installing the lidar on an expensive stiff platform to avoid extra measurement uncertainties, or significantly tilting up the lidar beam, which would introduce biases.

In the white box calibration, having access to reconstruction algorithms is mandatory. For commercial systems, these algorithms would need to be provided by the lidars' manufacturers to accredited calibration laboratories under confidentiality agreements. The inadequacy and/or uncertainties of the wind field reconstruction algorithms will need to be assessed, for example via Computational Fluid Dynamics and lidar simulator(s).

The presented methodology does not address the volume weighing process inherent to DWL. Further work on this question may thus be required for the white box methodology to achieve an even higher degree of genericity.

A controversial question remains: should the lidar measurements be corrected using the calibration results? Although the VIM provides a clear definition of the calibration and formally requires to apply the calibration relation (i.e., correct the measurements), lidars are currently calibrated in uncontrolled conditions. Indeed, atmospheric field measurements are the most representative of real-world lidar applications. In specific cases where lidars operate in conditions far from those of the calibration, correcting lidar measurements is not always advisable and artificially enlarging the uncertainties may be preferred. This could for instance require adding a classification uncertainty, if available.

8. Conclusions

In the present paper, we developed and demonstrated a generic calibration methodology for wind nacelle lidars. Two different possible calibration concepts were first identified, and their strengths and weaknesses discussed. The retained approach is the so called 'white box' calibration. It consists in calibrating all the inputs of the reconstruction algorithms applied by lidars to estimate wind

characteristics. In the 'white box' approach, the line-of-sight velocity calibration is central as all Doppler wind lidars first estimate the line-of-sight velocity and then use it for wind field reconstruction. Consequently, the white box calibration concept is generic since applicable to any lidar system with a similar procedure. In opposition, the 'black box' methodology is specific to each reconstructed parameter and requires expensive measurement setups.

The methodology to calibrate and assess the uncertainties of line-of-sight velocity measurements was described and illustrated by the examples of the calibration of two commercially developed lidars: a pulsed multi-beam system developed by *Avent Lidar Technology*; a continuous wave circularly scanning system developed by *ZephIR Lidar*. Calibration results from both lidars have proven to be consistent: the difference between the lidar-measured line-of-sight velocity and reference quantity value lies in the 0.5%–0.9% range. The excellent agreement observed is evidence of the feasibility of the line-of-sight velocity calibration. Uncertainties can be expected to vary between $\approx$3.5% at 3 m$\cdot$s^{-1} to $\approx$2% at 16 m$\cdot$s^{-1}.

Using a simple reconstruction algorithm applied to a two-beam nacelle lidar, inputs uncertainties were propagated to the reconstructed wind speed and relative direction. The assumed degree of correlation between uncertainty components proved to be of critical importance. Results also showed that uncertainties: on wind speed are of same magnitude as line-of-sight velocity uncertainties; on the relative wind direction decrease with the wind speed; are insensitive to the wind direction for normal turbine operational conditions.

Thanks to the generic calibration methodology, traceable lidar-estimated wind characteristics can be obtained and their uncertainties quantified.

Author Contributions: Antoine Borraccino was in charge of the research work and wrote the paper. Michael Courtney and Rozenn Wagner supervised the research work and the manuscript conception. All co-authors participated to the improvement of the manuscript.

References

1. Wagner, R.; Courtney, M.; Gottschall, J.; Lindelöw, P. Accounting for the speed shear in wind turbine power performance measurement. *Wind Energy* **2011**, *14*, 993–1004.
2. Peña, A.; Hasager, C.B.; Gryning, S.E.; Courtney, M.; Antoniou, I.; Mikkelsen, T. Offshore wind profiling using light detection and ranging measurements. *Wind Energy* **2009**, *12*, 105–124.
3. Wagner, R.; Pedersen, T.; Courtney, M.; Antoniou, I.; Davoust, S.; Rivera, R. Power curve measurement with a nacelle mounted lidar. *Wind Energy* **2014**, *17*, 1441–1453.
4. Borraccino, A.; Courtney, M. *Calibration Report for Avent 5-Beam Demonstrator Lidar*; Technical Report; DTU Wind Energy: Roskilde, Denmark, 2016.
5. Borraccino, A.; Courtney, M. *Calibration Report for ZephIR Dual Mode Lidar (Unit 351)*; Technical Report; DTU Wind Energy: Roskilde, Denmark, 2016.
6. Hardesty, R.M.; Weber, B.F. Lidar measurement of turbulence encountered by horizontal-axis wind turbines. *J. Atmos. Ocean. Technol.* **1987**, *4*, 191–203.
7. Lawrence, T.R.; Wilson, D.J.; Craven, C.E.; Jones, I.P.; Huffaker, R.M.; Thomson, J.A.L. A laser velocimeter for remote wind sensing. *Rev. Sci. Instrum.* **1972**, *43*, 512.

8.   Schlipf, D.; Rettenmeier, A.; Haizmann, F.; Hofsäß, M.; Courtney, M.; Cheng, P.W. Model based wind vector field reconstruction from lidar data. In Proceedings of the 11th German Wind Energy Conference (DEWEK 2012), Bremen, Germany, 7–8 November 2012.

9.   Sathe, A.; Banta, R.; Pauscher, L.; Vogstad, K.; Schlipf, D.; Wylie, S. *Estimating Turbulence Statistics and Parameters from Ground- and Nacelle-Based Lidar Measurements: IEA Wind Expert Report*; Grant No.: 0602-02486B; DTU Wind Energy: Roskilde, Denmark, 2015.

10. Vasiljevic, N. A Time-Space Synchronization of Coherent Doppler Scanning Lidars for 3D Measurements of Wind Fields. Ph.D. Thesis, DTU Wind Energy, Roskilde, Denmark, 2014.

11. Joint Committee for Guides in Metrology. *International Vocabulary of Metrology—Basic and General Concepts and Associated Terms (VIM)*; Technical Report, 200:2012; Bureau International des Poids et Mesures (BIPM): Sèvres, France, 2012.

12. Joint Committee for Guides in Metrology. *Evaluation of Measurement Data—Guide to the Expression of Uncertainty in Measurement*; Technical Report, 100:2008; Bureau International des Poids et Mesures (BIPM): Sèvres, France, 2008.

13. Gottschall, J.; Courtney, M.; Wagner, R.; Jørgensen, H.E.; Antoniou, I. Lidar profilers in the context of wind energy—A verification procedure for traceable measurements. *Wind Energy* **2012**, *15*, 147–159.

14. International Electrotechnical Commission (IEC). *Power Performance Measurements of Electricity Producing Wind Turbines*; IEC 61400-12-1 Ed. 2.0:CCDV; International Electrotechnical Commission: Geneva, Switzerland, 2015.

15. Wagner, R.; Courtney, M.S.; Pedersen, T.F.; Davoust, S. Uncertainty of power curve measurement with a two-beam nacelle-mounted lidar. *Wind Energy* **2016**, *19*, 1269–1287.

16. Joint Committee for Guides in Metrology. *Evaluation of Measurement Data—Propagation of Distributions Using Monde Carlo Method*; Technical Report; 101:2008; Bureau International des Poids et Mesures (BIPM): Sèvres, France, 2008.

17. Peña, A.; Floors, R.; Sathe, A.; Gryning, S.E.; Wagner, R.; Courtney, M.S.; Larsén, X.G.; Hahmann, A.N.; Hasager, C.B. Ten years of boundary-layer and wind-power meteorology at Høvsøre, Denmark. *Bound. Layer Meteorol.* **2016**, *158*, 1–26.

18. Borraccino, A.; Courtney, M.; Wagner, R. *Generic Methodology for Calibrating Profiling Nacelle Lidars*; Technical Report; DTU Wind Energy: Roskilde, Denmark, 2015.

19. Raach, S.; Schlipf, D.; Haizmann, F.; Cheng, P.W. Three dimensional dynamic model based wind field reconstruction from lidar data. *J. Phys. Conf. Ser.* **2014**, *524*, 012005.

20. Towers, P.; Jones, B.L. Real-time wind field reconstruction from LiDAR measurements using a dynamic wind model and state estimation. *Wind Energy* **2016**, *19*, 133–150.